Modeling of an injected gas laser

P. Even, K. Ait Ameur, and G. M. Stéphan
Laboratoire d'Optronique, Associé au Centre National de la Recherche Scientifique (EP001), ENSSAT, 6 rue de Kérampont, 22305 Lannion Cedex, France

(Received 22 July 1996; revised manuscript received 16 September 1996)

We develop a model to compute the line shape of an injected gas laser. The model describes the competition that occurs between the injected field and the usual resonant field of the laser, which are both considered as separate dynamic variables. A small signal stability analysis of the stationary solutions is used to study this competition: the laser field may be destroyed due to gain quenching by the injected field, which explains the frequency locking phenomenon. We give the connection with the standard Adler model. Theoretical and experimental results that describe the line shape inside or outside the locking range are given for the typical He-Ne laser operating at 3.39 μm. [S1050-2947(97)01902-1]

PACS number(s): 42.55.Lt, 42.55.Ah, 42.65.Pc

I. INTRODUCTION

One of the most spectacular phenomena observed in coupled lasers is frequency locking. This phenomenon is usually theoretically described by the so-called Adler model, which was initially developed for coupled electronic oscillators [1]. The phenomenon is well known in laser physics and widely used for many purposes, for instance, to stabilize the frequency [2], to lock the phase of separate lasers [3], to spectrally narrow the linewidth, to select the frequency of the injected laser [4], or to obtain single-mode operation [5,6]. It was first studied on He-Ne lasers [7] and later on all kinds of lasers such as CO_2 [4], argon [5], erbium [6], dye [8], Nd:YAG (where YAG denotes yttrium aluminum garnet) [9,10], or semiconductor lasers [11].

In the most simple experiment, one injects the light merging from a single-mode laser, called the master laser (ML), into the slave laser (SL) across an optical isolator. In this study we will also consider single-mode lasers. When both lasers are decoupled, their respective fields have different frequencies: the SL works at ω_1 and the ML at ω_2. Locking of the SL on ω_2 occurs when ω_1 and ω_2 are close enough and when the injected intensity is high enough. Here we will be interested in the injected laser output intensity when its length is scanned for a fixed frequency of the ML. It is this output that we will call ''line shape'' in the remaining of this paper.

Up to now, the theory of injected lasers has been aimed essentially at the description of locking conditions. The locked response is studied as a function of the amplitude of the injected signal, which is viewed as an additional pump mechanism. In Adler's model, the interpretation of the effect depends on a locking of the phase of the free running mode to that of the external signal [12]. However, an injected laser shows other peculiarities and the most important of them is its line shape as defined above. In fact, if a theory can describe the line shape it will necessarily describe the locking phenomenon because both phenomena are intrinsically linked. Up to now, it seems that such a theory does not exist and it is the aim of this article to present a model designed to compute this line shape and to include, in a synthetic way, various observable phenomena belonging to the physics of an injected laser.

Our motivation in achieving this goal was essentially to set up the basis for an alternative method to study injected lasers: we have noticed that in previous studies, the term that represents the losses of the cavity in the equations for the fields is taken as a constant, whatever the frequency of the injected field. This is in contrast with an ordinary Fabry-Pérot interferometer (FPI), where the transmitted or internal fields are strongly dependent upon frequency. Described in the following is that we have split the field into its two frequency-component parts and that each is taken as a dynamic variable with different frequency-dependent characteristics. This view should improve the precision of former studies.

It is our opinion that Adler's model does not give a convincing or a complete physical explanation of injected lasers, including the frequency locking phenomenon. Although it is widely used, it shows at least two failures: (i) it does not contain the most simple phenomenon embedded in the usual Airy function that describes the passive FPI when the active medium is removed from the slave laser and (ii) it cannot describe the nonlocked regime since its validity is justified only in the locked regime.

Our theoretical description of an injected laser corrects these drawbacks. Indeed, we consider the field in the SL to have two frequency components E_1 and E_2. E_1 is resonant and represents the normal SL eigenmode with a frequency ω_1. E_2 is generally nonresonant and builds up from the external signal injected at the frequency ω_2. Then we consider E_1 and E_2 as competing fields whose gains are coupled through saturation. Their time evolution is described by two complex rate equations that show two kinds of stationary solutions: (i) E_1 and $E_2 \neq 0$ correspond to the unlocked regime and (ii) $E_1 = 0$ and $E_2 \neq 0$ correspond to the locked regime. A stability analysis of these steady-state solutions shows that the locked regime occurs when the gain of the resonant field is quenched by the injected field. It clearly appears that the passage from the unlocked to the locked regime is due to the competition originating from the cross saturation between the two components E_1 and E_2. The proposed model is thus valid inside and outside the locking

range. It also describes correctly the passive FPI and gives a good physical explanation of the locking process. It is illustrated in the simpler case of a gas laser where the adiabatic elimination of fast variables simplifies the equations, but the basic idea of the two-field components with different characteristics is general and may be extended to other lasers. For instance, the theory of instabilities of class-*B* injected lasers [13] can be rewritten with the use of these two dynamical variables, which would give rise to five coupled nonlinear equations instead of three in this particular case. However, this view should not be extended to every class of injected lasers, for example, the laser with phase-conjugate optical feedback [14], where the injected frequency is defined by the same laser.

The idea of competition between two fields that is developed here is not new: it has already been published independently by Tang and Statz [15] and Boikova and Fradkin [16] 30 years ago and expressed again in more recent papers, for instance, in Refs. [17–19]. However, in these papers, the theory is not adapted to compute the line shape. Indeed, in Refs. [15,16,20] the loss term is the same for both the resonant and the injected fields and thus a precise study of the competition cannot be undertaken. It is probably this weakness that prevented the success of the early theories and oriented toward the use of Adler's model. The different idea here is to use a different term to represent the cavity losses for the two frequency components: this allows us to make the connection to the Airy function of an empty cavity where the frequency-dependent loss is known. This is also coherent with a calculation developed [21] to compute the variation undergone by the laser line shape from below to above threshold.

We have chosen to test our model on a He-Ne laser operating at 3.39 μm because of its simplicity. There are few or no experimental results in the literature about the influence of the amplitude and frequency of the injected signal on the SL line shape. An example can be found in Ref. [22], but the theory given there was again not designed to describe the line shape. This lack of results is probably due to the absence of correct models able to describe, for instance, the intensity peak that is added to the SL line shape around the injected frequency. Here we will see that experimental and calculated line shapes agree nicely.

The paper is organized as follows. In Sec. II we briefly recall Adler's model and delimit its restrictions. In Sec. III we establish the equations of the present model. In Sec. IV we solve for the steady-state solutions and study their stability. Experimental and theoretical line shapes are given in Sec. V.

II. ADLER'S MODEL OF INJECTION LOCKING

In this section we recall the standard method used to describe the laser with an injected signal. While this method is described in many laser textbooks [12], we have chosen to include it here rather than in an appendix in order to review some definitions and notions in a familiar context and to provide a linear path to the reader. A typical example of this theory is given in Refs. [23,24], where a few effects have been predicted: for instance, pulsing when the system is not locked or bistable phenomena. It is important to note that, in this usual approach, the injected signal operates like a source term only and not as a dynamical variable.

In this model, the time evolution of the SL eigenfield

$$E_c(t)=\mathcal{E}_c(t)\exp[i(\omega t+\phi_c(t))] \tag{1}$$

is due to a number of contributions, namely, the cavity losses represented by a decay rate γ_c and two source terms: the atomic polarization P and the external field

$$E_{\rm inj}(t)=\mathcal{E}_{\rm inj}(t)\exp\{i[\omega t+\phi_{\rm inj}(t)]\} \tag{2}$$

injected at a rate $\gamma_{\rm inj}$. ω is simply a reference for the frequency: the instantaneous frequencies depend also upon the derivatives of $\phi_c(t)$ and $\phi_{\rm inj}(t)$. We assume that the slave laser cavity of length d is made up of two identical mirrors of reflectivity R and transmission $T=1-R$. The rates γ_c and $\gamma_{\rm inj}$ can be written as

$$\gamma_c=c/2d\ \ln(1/R)\cong c/2d(1-R),\quad \gamma_{\rm inj}=c/2d\sqrt{T}.$$

In the following, $\Delta_c=c/2d$ denotes the free spectral range of the cavity and the loss term $p=-\ln(R)\cong 1-R$ when R is close to unity. Equations of evolution are

$$\frac{d\mathcal{E}_c(t)}{dt}=[\alpha-\gamma_c-\beta\mathcal{E}_c^2(t)]\mathcal{E}_c(t)+\gamma_{\rm inj}\mathcal{E}_{\rm inj}(t)\cos[\phi_c(t)-\phi_{\rm inj}(t)], \tag{3a}$$

$$\frac{d\phi_c(t)}{dt}=(\omega_0-\omega)-\gamma_{\rm inj}\frac{\mathcal{E}_{\rm inj}(t)}{\mathcal{E}_c(t)}\sin[\phi_c(t)-\phi_{\rm inj}(t)]. \tag{3b}$$

Here ω_0 is the oscillation frequency of the slave laser without injection in which pulling and pushing effects have been included. The frequency-dependent quantities α and β are, respectively, the gain and self-saturation coefficients.

The steady-state solution of Eqs. (3a) and (3b) corresponding to the particular case of an empty cavity ($\alpha=\beta=0$) should describe the response of a Fabry-Pérot interferometer. However, this is not the case, for one finds, when R is close to unity,

$$\left(\frac{\mathcal{E}_c}{\mathcal{E}_{\rm inj}}\right)^2\cong\frac{T}{(1-R)^2}\frac{1}{1+[(\omega-\omega_0)/\Delta_c(1-R)]^2}. \tag{4}$$

Equation (4) describes correctly the response of a passive Fabry-Pérot interferometer only inside the small frequency interval around resonance where the Airy function reduces to a Lorentzian. This usual Airy function writes

$$\left(\frac{\mathcal{E}_c}{\mathcal{E}_{\rm inj}}\right)^2\cong\frac{T}{(1-R)^2}\frac{1}{1+\dfrac{4}{(1-R)^2}\sin^2\left(\dfrac{\omega-\omega_0}{2\Delta_c}\right)}. \tag{5}$$

The underlying cause of this inadequate description of the FPI is inherent to the phase-amplitude equations (3a) and (3b), which have a steady-state solution only if $d\phi_c(t)/dt=0$. This condition can be fulfilled only when the injected frequency is close to the resonance frequency of the FPI.

When the frequency ω of the injected signal is close enough to ω_0, the slave laser is locked and oscillates with the injected frequency. If the phase of the injected signal is assumed as a constant reference, the locking condition is written as

$$\omega-\omega_0+\omega_m\sin(\phi_c)=0 \tag{6}$$

with

$$\omega_m=\gamma_{\rm inj}\frac{\mathcal{E}_{\rm inj}}{\mathcal{E}_c}. \tag{7}$$

Taking into account that the sine function is bounded by -1 and $+1$, the locking condition writes

$$-\omega_m\leqslant(\omega-\omega_0)\leqslant\omega_m, \tag{8}$$

which gives the locking range

$$\Delta\omega_{\rm lock}=2\omega_m=2\gamma_{\rm inj}\mathcal{E}_{\rm inj}/\mathcal{E}_c \tag{9}$$

extending from $(\omega_0-\omega_m)$ to $(\omega_0+\omega_m)$. Outside this interval there is no steady-state solution for the phase ϕ_c and Adler's model cannot describe the laser with an injected signal. This treatment of the frequency locking phenomenon is absolutely opaque as for its physical origin.

To conclude this section one should note that numerous experiments with various lasers confirm the linear variation of the locking range with the amplitude of the injected signal [6,7,9] and this is probably why Adler's model is so widely used. Nevertheless, one notes that expression (9) tells us that $\Delta\omega_{\rm lock}\neq0$ when the injected field $\mathcal{E}_{\rm inj}\neq0$. Sometimes this is not experimentally verified: a threshold for $\mathcal{E}_{\rm inj}$ has been observed below which locking does not occur [6,7,9]. In fact, a bistable domain appears for small values of $\mathcal{E}_{\rm inj}$, as will be seen below.

III. MODEL OF THE INJECTED LASER

In Adler's model, the field E inside the monomode slave laser is supposed to have a single-frequency component, which is valid *inside* the locking range. Here we take the opposite point of view, i.e., we assume that E generally has two components, one with the eigenfrequency ω_1 and the other with the ML frequency ω_2. This assumption is valid outside the locking range as well and enables a more powerful theory. As noted above, this idea was originally given independently by Tang and Statz [15] and Boidkova and Fradkin [16]. For the moment, we limit ourselves to fields that are linearly polarized along the same direction. One writes

$$E=E_1e^{i\omega_1t}+E_2e^{i\omega_2t}, \tag{10}$$

where E_1 and E_2 are complex and represent the slowly varying part of the mean-field components. In the following we will neglect the field components having frequencies such as $2\omega_1-\omega_2$, which are generated through nonlinear phenomena, because they are weak and not resonant in the case considered here. The signal from the ML is characterized by an amplitude $\mathcal{E}_{\rm inj}$ incident on the SL. $\mathcal{E}_{\rm inj}$ creates, inside the laser, another, nonresonant field, which we denote E_2. E_2 has the same frequency as $\mathcal{E}_{\rm inj}$, but a different phase and a different amplitude. This is exactly the same phenomenon that happens when an external field creates another field inside an empty Fabry-Pérot cavity. The amplitude and phase are separated in E_2 and in E_1:

$$E_2=\mathcal{E}_2e^{i\varphi_2}, \tag{11}$$

$$E_1=\mathcal{E}_1e^{i\varphi_1}. \tag{12}$$

The phase of the external signal will be taken later as the phase reference for both components $E_{1,2}$. The rate of change of the two field components is determined by the round-trip method [21,25,26], where the effect of the active medium is taken into account: we thus introduce the saturated susceptibility $\chi(\omega)=\chi'(\omega)+i\chi''(\omega)$ for the mean field. Following this method, the rate equations for the components E_1 and E_2 are then written as

$$\frac{\partial E_1}{\partial\tau}=-E_1[1-e^{-p}e^{-2ik_1d}], \tag{13}$$

$$\frac{\partial E_2}{\partial\tau}=-E_2[1-e^{-p}e^{-2ik_2d}]+s, \tag{14}$$

where τ is the time expressed in round-trip time units $(1/\Delta_c)$ and $e^{-p}=R$. With this unit, s represents the rate with which the external field enters into the slave laser:

$$s=\sqrt{T}\mathcal{E}_{\rm inj}. \tag{15}$$

The source term corresponding to spontaneous emission has been neglected here as compared to s [21]. The wave number k is related to the frequency ω and the susceptibility χ by the relation

$$k(\omega)\approx\frac{\omega}{c}\left(1+\frac{\chi(\omega)}{2}\right). \tag{16}$$

Subscripts 1 and 2, attributed to the wave numbers in Eqs. (13) and (14), mean that k is evaluated, respectively, for the frequencies ω_1 and ω_2. From Eq. (16) one sees that $k(\omega)$ is complex and for convenience we will separate the phase and amplitude contributions of $\exp(-ik_{1,2}d)$ in Eqs. (13) and (14), which become

$$\frac{\partial E_1}{\partial\tau}=-E_1\left[1-e^{-i\Phi_1}\exp\left(-p+\frac{\omega_cd}{c}\chi_1''\right)\right], \tag{17}$$

$$\frac{\partial E_2}{\partial\tau}=-E_2\left[1-e^{-i\Phi_2}\exp\left(-p+\frac{\omega_cd}{c}\chi_2''\right)\right]+s, \tag{18}$$

where $\omega_c=2N\pi\Delta_c$ is the resonance frequency of the bare cavity. Strictly, one should write $\omega_{1,2}$ instead of ω_c in Eqs. (17) and (18): this is necessary in the phase term, but not for the gain. The round-trip accumulated phases $\Phi_{1,2}$ for each component in the SL are expressed as

$$\Phi_{1,2}=\frac{\omega_{1,2}}{\Delta_c}\left[1+\frac{\chi'_{1,2}}{2}\right]. \tag{19}$$

The phase term disappears from Eq. (17) since the SL eigenfield is resonant: $\Phi_1=2N\pi$ and $\exp(i\Phi_1)=1$. On the contrary, the phase term in Eq. (18) $\exp(i\Phi_2)\neq 1$ since the injected signal is not resonant and this is the different feature of our model. This means, in particular, that the loss levels experienced by the components E_1 and E_2 are different. Moreover, the effective loss associated with the component E_2 is frequency dependent even though that associated with E_1 is constant. This can be understood if we remember the behavior of an empty, passive Fabry-Pérot cavity depicted by Eq. (5). In that case, a nonresonant field is characterized by a decay rate $\Delta_c[1-R\cos(\Delta\omega/\Delta_c)]$, while a resonant field is characterized by $\Delta_c[1-R]$. Here $\Delta\omega$ is the detuning between the injected and resonant frequencies. In the case of a laser the phase depends also upon the saturated susceptibility and thus the theory contains a phase-coupling term. Related to this point, we have to recall the treatment given in Refs. [15,16]. Here the two components of the field are characterized by the same loss term. Lamb's equations are only adapted to describe resonant fields (modes): for instance, they cannot be reduced to the description of the empty cavity by removing the active medium, thus they cannot be applied to the problem of an injected laser with a nonresonant field.

Before we proceed further, we note that one can verify that Eq. (18) describes correctly the passive Fabry-Pérot interferometer when the susceptibility $\chi(\omega)$ reduces to zero. We look for the steady state of E_2, knowing that $E_1=0$ in this case. Doing that, we find a result identical to Eq. (5).

The frequency dependence of the saturated susceptibility $\chi(\omega)$ depends on the considered line profile, which can be Lorentzian (homogeneous broadening), Gaussian (inhomogeneous broadening), or a mixture of both (Voigt). We have considered the latter case and the emission line shape is described by the complex plasma-dispersion function $Z(\zeta)$. The expression of the saturated susceptibility is given in Appendix A. The complex variable ζ is defined as

$$\zeta=X+iY, \tag{20}$$

where Y represents the ratio of the homogeneous (Γ_L) to the inhomogeneous (Γ_G) widths of the laser transition

$$Y=\frac{\Gamma_L}{\Gamma_G} \tag{21}$$

and X is the reduced frequency defined by

$$X=\frac{\omega-\omega_0}{\Gamma_G}. \tag{22}$$

The real and imaginary parts of Eqs. (17) and (18) can be written as

$$\frac{d\mathcal{E}_1}{d\tau}=-\mathcal{E}_1[1-\exp(-p+\rho_1^i)], \tag{23a}$$

$$\frac{d\varphi_1}{d\tau}=0 \tag{23b}$$

$$\frac{d\mathcal{E}_2}{d\tau}=-\mathcal{E}_2[1-\cos(\Phi_2)\exp(-p+\rho_2^i)]+s\cos(\varphi_2), \tag{23c}$$

$$\frac{d\varphi_2}{d\tau}=-\sin(\Phi_2)\exp(-p+\rho_2^i)-\frac{s}{\mathcal{E}_2}\sin(\varphi_2), \tag{23d}$$

with $\rho_{1,2}=pg[\alpha_{1,2}-\beta_{1,2}I_{1,2}-\theta_{12,21}I_{2,1}]$. g is the reduced gain normalized at threshold. Superscripts r and i stand for the real and imaginary parts of the quantities. Subscripts 1 or 2, assigned to the atomic variables α, β, and θ, refer to quantities that are evaluated for the frequency ω_1 or ω_2, respectively. The intensity associated with each signal is defined as the square of the field amplitude, i.e., $I_{1,2}=\mathcal{E}_{1,2}^2$. α represents the complex gain where the imaginary part describes the low-signal gain and the real part describes pulling effects. β and θ are the complex self- and cross-saturation coefficients. The quantities α, β, and θ are frequency dependent and their expressions are given in Appendix A.

Examination of Eqs. (23) shows that the two field components are coupled through saturation effects. In particular, the effective gain experienced by each component depends on the intensity of the other. This effective gain writes

$$-p+\rho_{1,2}^i=-p+pg[\alpha_{1,2}^i-\beta_{1,2}^iI_{1,2}-\theta_{12,21}^iI_{2,1}]. \tag{24}$$

One expects that the energy exchange between these components plays an important role in the behavior of the laser with an injected signal and that a competition may occur between them. It is also clear that the cumulated phase experienced by both components depends on the intensity of the other and thus mutual frequency push-pull effects will appear. We will not study such effects in the present work. The next step is to determine the steady-state solutions of Eqs. (23) and study their stability.

IV. STEADY-STATE AND STABILITY ANALYSIS

Since we are interested in the steady-state operation of the SL, the time derivatives are set to zero and the four Eqs. (23) are solved for $\mathcal{E}_1$, $\mathcal{E}_2$, φ_1, and φ_2. After some straightforward algebra Eqs. (23) can be cast into

$$I_1[1-\exp(-p+\rho_1^i)]^2=0, \tag{25a}$$

$$I_2[1-2\cos(\Phi_2)\exp(-p+\rho_2^i)+\exp 2(-p+\rho_2^i)]=s^2, \tag{25b}$$

$$\cos(\varphi_2)=\frac{\sqrt{I_2}}{s}[1-\cos(\Phi_2)\exp(-p+\rho_2^i)], \tag{25c}$$

$$\sin(\varphi_2)=-\frac{\sqrt{I_2}}{s}\sin(\Phi_2)\exp(-p+\rho_2^i). \tag{25d}$$

The set of equations (25) shows two groups of solutions, for the amplitude of the two fields:

$$\mathcal{E}_1=0,\quad \mathcal{E}_2\neq 0\quad (\text{case } A),$$

$$\mathcal{E}_1\neq 0,\quad \mathcal{E}_2\neq 0\quad (\text{case } B).$$

Case A. The first group of solutions, which will be labeled *A*, corresponds to the locked regime, i.e., the laser oscillation is quenched by the external signal. This can be easily understood from Eq. (25a) with the expression (24) for the effective gain. If the intensity I_2 is high enough to force the term $(-p+\rho_1^i)$ toward negative values, the component $\mathcal{E}_1$ is destroyed because it experiences no gain. In other words, the locking of the laser has to be closely associated with the cross saturation (at least, at first sight). In the locked regime, the output of the slave laser corresponds to an injected signal that is amplified by the regenerative gain, resulting from the nonoscillating slave laser.

Case B. The second group of solutions, labeled *B*, indicates a coexistence of the two uncorrelated components with frequencies ω_1 and ω_2, i.e., the slave laser is not locked.

These two groups of solution can be exclusive of each other, but they can overlap as well, depending on the experimental conditions. One sees that, because of the nonlinearity of the equations, several solutions for the intensity are possible, for a given parameter set. The main control parameters in an injected laser experiment are the gain g and the optical length of the slave laser, the frequency ω_2, and the strength of the injected signal. One should note that, for the same length, one can have several solutions for the frequency of the SL. This is because the round-trip phase $\Phi_1=2N\pi$ depends upon ρ_1^r, which itself depends upon the intensities. As soon as there are several possible solutions for the intensities for a given length, there are also several possible frequencies.

Thus one is led to study the stability of the steady-state solutions of Eqs. (25) for different sets of control parameters. For instance, in our experiment, we scanned the SL length with a constant injected signal. In the following we will perform a stability analysis of the steady-state solutions: the intensity of the slave laser inside and outside the locking range can be found with this method and this is what we want to compare with the experimental observations. One should be well aware that three dynamical variables ($\mathcal{E}_1$, $\mathcal{E}_2$, and φ_2) govern the system and thus there are three Lyapunov exponents for each stationary solution. Following the experiment, one has to choose the proper path in the complicated phase domain. In the present work, we have chosen to limit ourselves to the particular situation where the control parameter is the optical length of the slave laser. However, it should be noted that the theoretical results also describe other effects such as jumps of intensity from solution *A* (*B*) to solution *B* (*A*) accompanied by hysteresis effects. These bistable effects can be observed with the intensity of the master laser as the control parameter, for fixed frequencies of both the ML and the SL. They will be described in detail in another paper.

Before we proceed further, it is important to characterize the strength of the injected signal. This is done by the injection factor η defined as the amplitude of the injected field normalized by the same value as that used for the SL field (see Appendix A).

A. Steady state: Case A

Here the SL eigenfield is switched off by the injected signal and this is the most simple situation because $I_1=0$. Now, depending on the values of the parameters, the set of equations (25) gives one or three real and positive solutions for I_2. Figure 1 shows a plot of the solution I_{2A} as a function of the injected amplitude field for two values of the reduced frequency X_2 of the master laser: $X_2=0$ [Fig. 1(a)] and $X_2=0.003$ [Fig. 1(b)]. In both cases the SL frequency is at line center, i.e., $X_1=0$, which corresponds to the laser length d_0. We will call δd the variation of this length with respect to d_0. The case $X_1=0$ leads to simpler numerical calculations because some dispersive effects vanish. As a first comment, one sees that the length (i.e., the frequency) of the slave laser plays a role, even though $I_{1A}=0$. This becomes clear if one examines the phase term Φ_2, which is given by Eq. (19) in which the length appears inside Δ_c:

$$\Phi_2=\frac{\omega_2}{\Delta_c}\left[1+\frac{\chi_2'}{2}\right]=\frac{2d\omega_2}{c}\left[1+\frac{\chi_2'}{2}\right].$$

The curve in Fig. 1(b) shows that the solution I_{2A} can be single or triple valued depending on the strength of the injected field. This could mean bistability in the intensity response of the SL if solution *A* were alone. This is a consequence of Eqs. (25), which, for $I_1=0$, describe the evolution

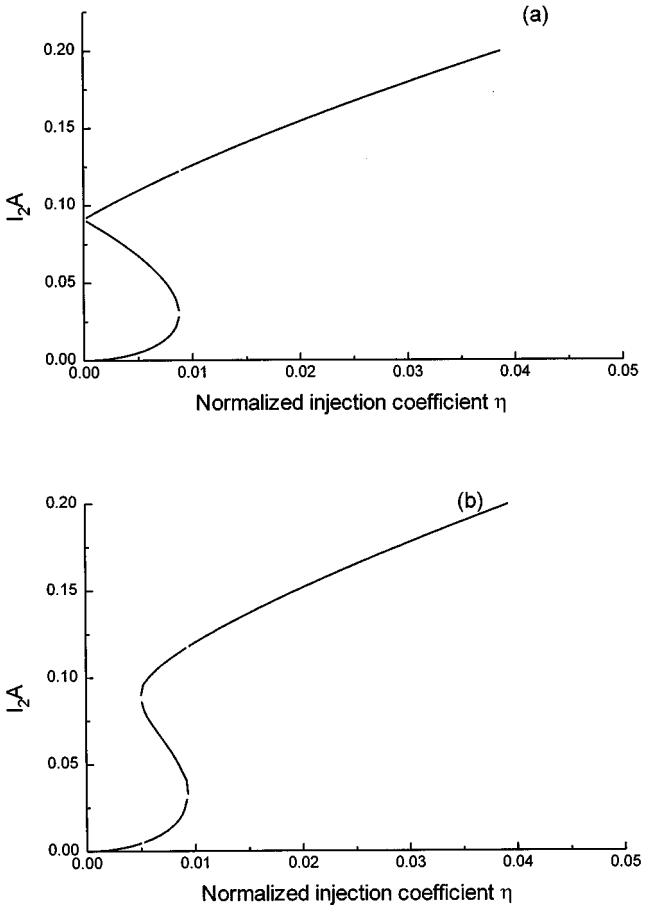

FIG. 1. Intensity I_{2A} inside the slave (here locked) laser vs the normalized injected intensity η when the normalized frequency $X_1=0$ (frequency of the slave laser at line center). In the numerical calculations, we took $Y=0.5$, $d_0=45$ cm. These values have been used in the computations leading to Figs. 1–6. (a) $X_2=0$. (b) $X_2=0.003$. It should be noted that the stability analysis reveals that these stationary solutions can be unstable.

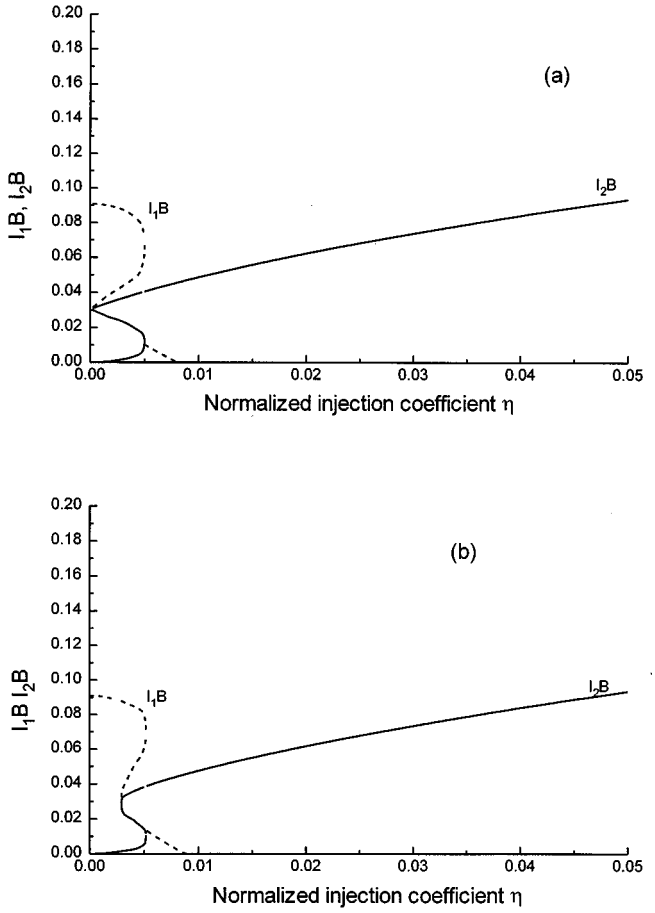

FIG. 2. Intensities of the field components I_{1B} and I_{2B} inside the slave (here unlocked) laser vs the normalized injected intensity η for the same control parameters as in Fig. 1. Dashed lines, I_{1B}; continuous lines, I_{2B}. Again these solutions can be unstable.

of an optical signal injected into a Fabry-Pérot cavity filled by a resonant saturable medium. The variations of I_{2A} alone with the amplitude of the injected field show a hysteretic cycle whose width decreases when the detuning δX increases. If the input frequency is resonant, i.e., $\delta X=0$, the curve touches the I_{2A} axis [Fig. 1(a)] and moves away from it for $\delta X>0$ as shown in Fig. 1(b). This effect can also be found from Adler's model and has already been reported in the literature [23]. It is also coherent with what happens in the ordinary dispersive bistability. However, as we will see, the lower and the middle branches are unstable here because one has to consider the set of the three Lyapunov exponents simultaneously and thus the hysteresis cycle of I_{2A} is not experimentally observable alone.

B. Steady state: Case B

The field in case B, contrary to case A, is characterized by the coexistence of the laser and the injected components. Figure 2 displays the variations of the intensities I_{1B} and I_{2B} as a function of the injection factor for $X_2=0$ and $\delta d=0$ [Fig. 2(a)] and $X_2=0.003$ and $\delta d=0$ [Fig. 2(b)]. As in Fig. 1, one can again observe S-shaped curves that will introduce some complexity to the phenomenon. At this point, we do not yet know which solution A (locked) or B (nonlocked) will be chosen by the laser.

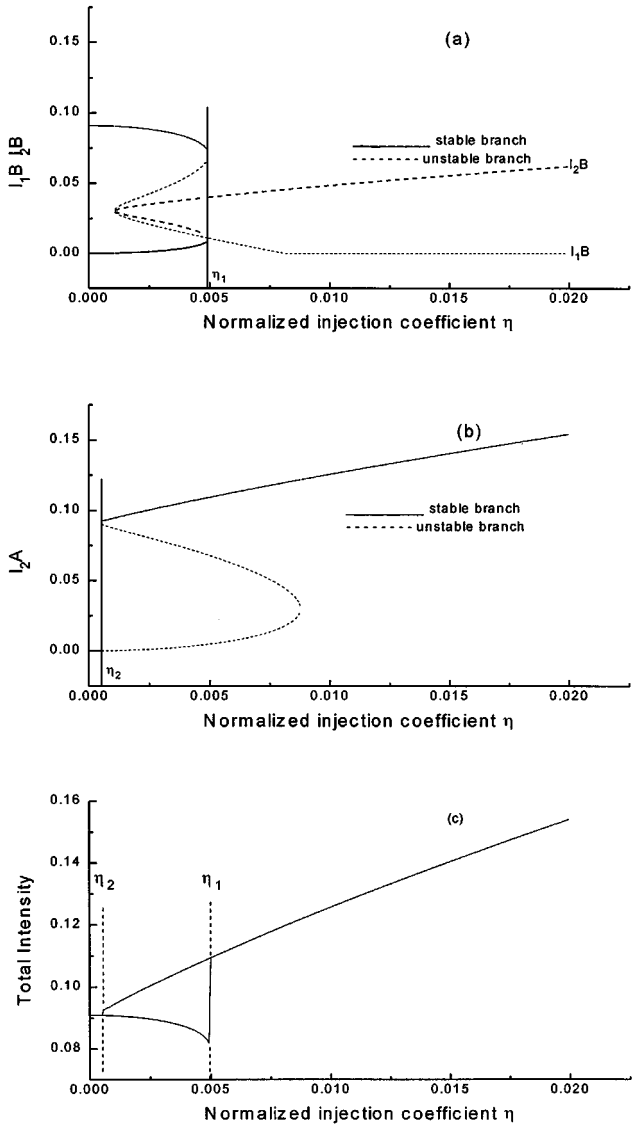

FIG. 3. Intensities (a) I_{1B} and I_{2B} in the unlocked regime, (b) I_{2A} in the locked regime, and (c) total measurable intensity showing the bistable domain between the limits η_1 and η_2 vs the injected intensity. Here $X_2=0$ and the variation $\delta d=0.001$ μm of the SL length with respect to the line center.

In order to answer this question, one has to study the stability of the stationary solutions. This is done by making a standard small signal linear stability analysis of the steady-state solutions A and B. This stability is governed by three Lyapunov exponents associated with the dynamical variables $\mathcal{E}_1$, $\mathcal{E}_2$, and φ_2. The existence of at least one Lyapunov exponent with a positive real part means that the steady state under consideration is unstable. The calculation of these Lyapunov exponents is standard and details are given elsewhere [28]. The main steps and an example are indicated in Appendix B.

Figure 3 describes a hysteresis cycle [Fig. 3(c)] for the total SL intensity that can be observed when the injected power η is increased and then decreased for a fixed frequency of both lasers. In this example, we have taken $X_2=0$ and $\delta d=0.001$ μm. When $\delta d=0.001$ μm, one can note that there are three values of the frequency X_1 (which are around

0.001 23, corresponding to a detuning of 180 kHz). Figures 3(a) and 3(b) display the intensities in the unlocked case [Fig. 3(a)], and in the locked case [Fig. 3(b)]. In Figs. 3(a) and 3(b) vertical lines have been drawn separating unstable and stable regions as a function of η. This has been done after examination of the numerical values of the Lyapunov coefficients. For small values of η, on the left of η_1 [Fig. 3(a)], the calculated Lyapunov exponents tell us that the upper (I_{1B}) and the lower branch (I_{2B}) of solution B are stable (unlocked laser). They also tell us that, on the right of point η_2 [Fig. 3(b)], the upper branch of solution A is stable. Thus one sees that an increase of η starting from $\eta=0$ brings the laser from the unlocked regime [Fig. 3(a)] into the locked regime at η_1. Now a decrease of η from upper values, i.e., in the locked region [Fig. 3(b)], forces the laser to jump to the unlocked solution for η_2. Thus the bistability range is, for this frequency, $\Delta\eta=\eta_2-\eta_1$. Let us note that this hysteresis effect is frequency dependent: $\Delta\eta$ decreases when δX increases. The output intensity of the SL is proportional to the total intensity I_T available inside the cavity: it is proportional to $I_T=I_{2A}$ in case A and to $I_T=I_{1B}+I_{2B}$ in case B. The curve in Fig. 3(c) shows the predicted observable intensity as a function of η.

Calculated line shapes can also be obtained from the preceding analysis. Graphs in Fig. 4 show an example of the total intensity I_T of the slave laser [Fig. 4(a)] together with the variations of I_1 [Fig. 4(b)] and I_2 [Fig. 4(c)] as a function of the SL length. The resonant frequency is at line center and the injected intensity is high enough to avoid any bistability (η=4%). As the eigenfrequency of the slave laser comes closer to the injected frequency, one sees a collapse of the intensity I_1 [Fig. 4(b)] and a simultaneous increase in I_2 [Fig. 4(c)]. The interval of length of the slave cavity for which the intensity I_1 vanishes corresponds to the locking range. The line shape of the slave laser I_T [Fig. 4(a)] shows an intensity peak surrounded by two dips. This peak is a sensitive function of the injection factor as shown in Fig. 5, where the line shape is drawn for four values of η. One should have a double-valued curve for small values of η. We have drawn here the solution with the lower intensity only, leaving the complete study of bistable effects for another paper.

Another interesting case, not studied in the literature, is the line shape of the slave laser when the frequency of the injected signal is not at line center. Such a situation is depicted in the curves in Fig. 6, showing a similar behavior as in Fig. 5, but with asymmetric peaks and dips.

The main result of Adler's model concerns the locking range, which was found to increase linearly with the injection factor, as shown in Eq. (9) and observed experimentally by several authors [6,7]. Here one can define the locking range $\Delta\omega_{\text{lock}}$ in a natural way based on the stability analysis: $\Delta\omega_{\text{lock}}$ is the frequency domain where at least the real part of one Lyapunov exponent associated with solution B is positive (for a given set of control parameters). It is represented in Fig. 7 for two values of the reduced gain g of the slave laser (g is normalized to threshold). It should be recognized that (i) the variation of the locking range with the amplitude of the injected signal is globally linear and (ii) the frequency locking mechanism can have a threshold and gain dependence that are not expected from Adler's model. This threshold has already been experimentally observed [6,27].

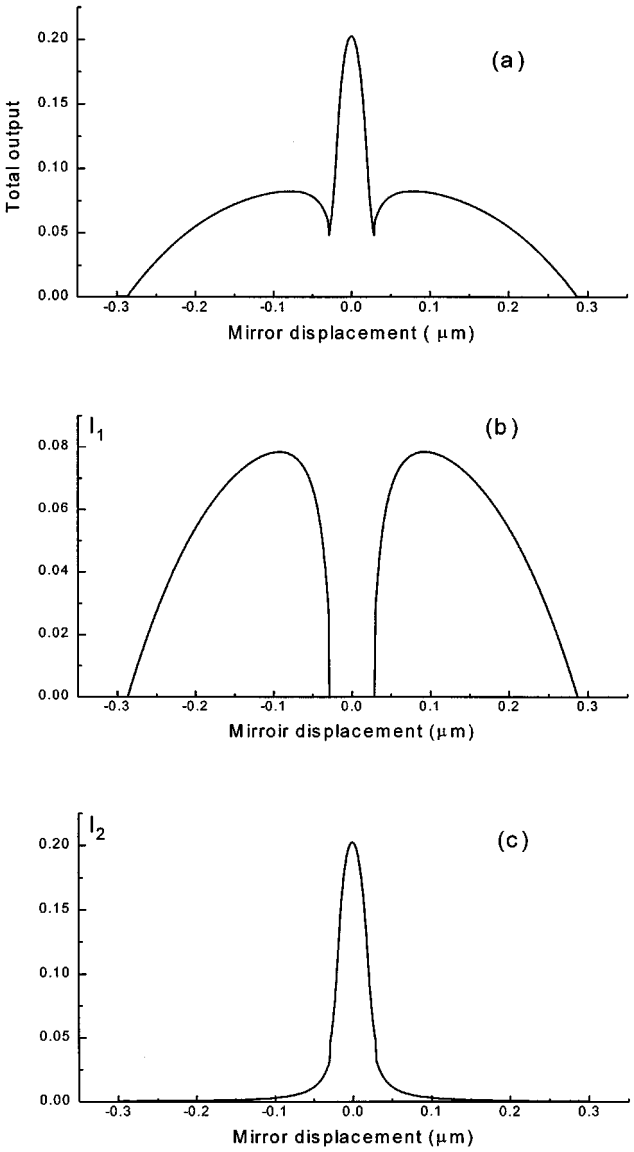

FIG. 4. Theoretical curves showing (a) the total intensity of the slave laser as a function of its length, (b) the intensity of the SL eigenmode, and (c) the intensity of the component corresponding to the injected signal. Here the gain $g=1.1$ and the laser is outside the bistability range, $\eta=0.04$. It should be noted that the frequency does not change inside the locking region where it is fixed by the master laser and two frequency components exist outside this domain.

In the next section we compare the theoretical results with experimental line shapes.

V. EXPERIMENTAL OBSERVATIONS

The experiment consists of two single-mode He-Ne lasers, sketched in Fig. 8, working on the same linear polarization at the wavelength $\lambda=3.39$ μm. The plasma tubes are homemade: the bore diameter is 3.5 mm, their length is 30 cm, and the total pressure is 2 Torr with a ratio $He:Ne^{20}=5:1$. The master laser is coupled into the slave laser through an optical isolator to prevent any optical feedback from the SL to the ML. Both the master and slave lasers are working on a single longitudinal and transverse mode. The

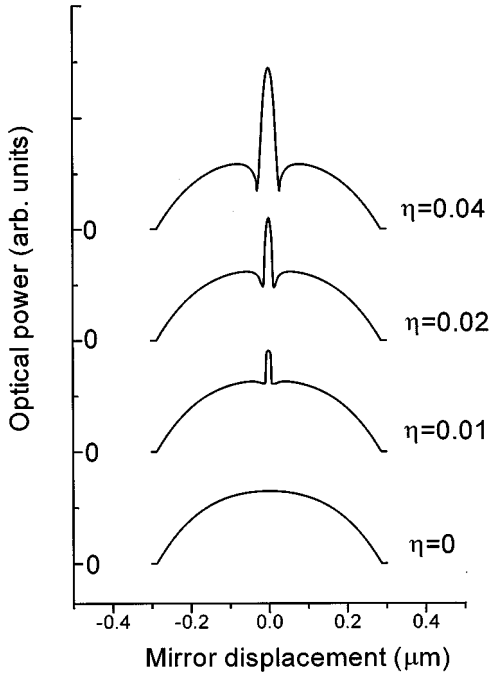

FIG. 5. Calculated line shape of the slave laser with increasing injection factor for $X_2=0$.

output mirror of the slave laser is held by a piezoelectric transducer (PZT) that allows the slave laser frequency to be swept freely. The adjustment of the master laser frequency is also done by a PZT, holding the rear mirror.

The object of the experiment is to measure the SL line shape, i.e., its intensity as a function of its optical length and the locking range for different parameters, which are the master laser frequency, the amplitude of the injected signal, and the gain of the slave laser or, more precisely, the discharge current in the slave laser. The first point to be discussed here is the strength of the coupling between the master and slave lasers. The incident power P_{in} at the entrance of the SL can be expressed as

$$P_{\text{inj}}=T_i K_G P_M ,$$

where P_M is the output power of the master laser, T_i is the transmission of the isolator made up of two calcite polarizers and a YIG crystal (where YIG denotes yttrium iron garnet), and K_G is a geometrical factor, less than unity, accounting for the geometrical overlap of the incident beam and the laser mode, both in the tranverse and longitudinal directions. For a given experiment, the value of K_G changes with respect to alignment. That makes experimental measurements on injected lasers difficult to reproduce quantitatively. We note that our experiment has not been designed to allow for any very precise control on K_G.

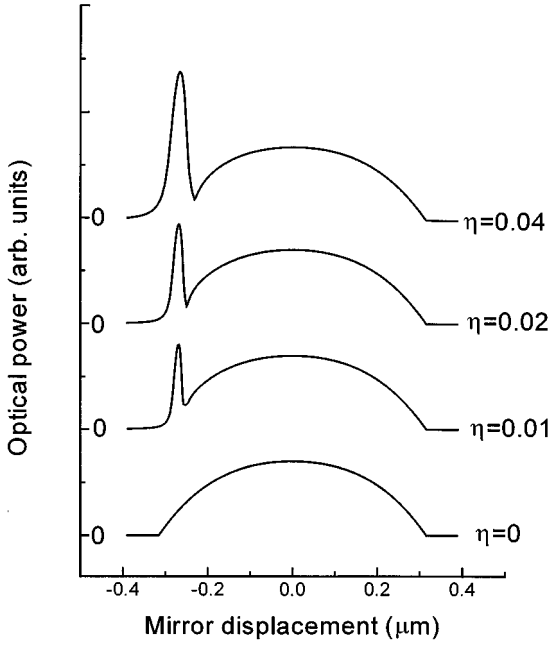

FIG. 6. Evolution of the calculated line shape of the slave laser with increasing injection factor for $X_2=0.3$.

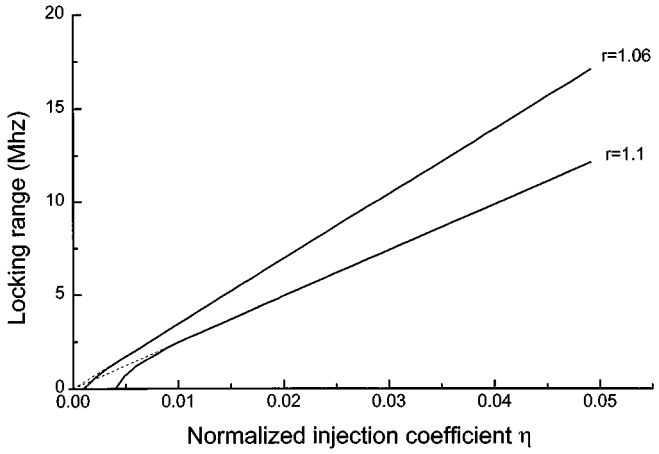

FIG. 7. Theoretical locking range as a function of the injection factor for two values of the gain of the slave laser. The upper branch crosses zero and the lower branch shows a threshold.

Experimental curves in Fig. 9 display the evolution of the SL line shape for different values of the injection factor when the injected frequency corresponds to the center of the Ne line. As in the theoretical results Fig. 5, an intensity peak appears around the injected frequency. This peak may be considered as an extension of the Airy function for the injected laser. It appears because the energy of the active medium is concentrated only in a single frequency component, while outside the locking range, it is split into two mutually incoherent fields. The shape of the intensity peak evolves according to the strength of the injected signal. Indeed, one sees that dips grow on both sides of the peak for higher injection levels. The case of the injection on one side of the slave laser line is shown in Fig. 10. The comparison of these experimental observations with the line shapes of Figs. 5 and 6 shows good agreement between our theoretical and experimental results.

VI. CONCLUSION

In this paper we have reexamined the early idea given by Tang and Statz [15], which states that the frequency locking phenomenon in injected lasers results from gain quenching by the imposed field. For this purpose, we have written two

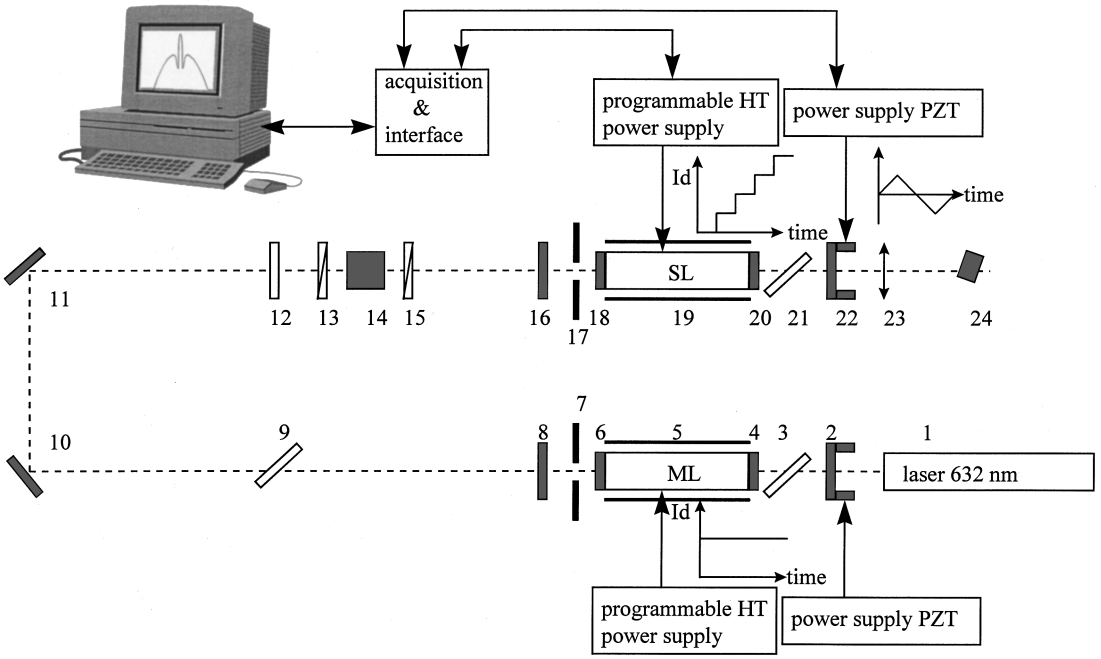

FIG. 8. Experimental setup: ML, master laser; SL, slave laser; 1, alignment laser; 2-22, piezoceramic transducer and laser mirror; 3-21, rotatable plates to control light polarization; 4-6-18-20, plates closing the laser tube; 5-19, μ metal shieldings; 7-17, apertures to obtain single-frequency lasers; 8-16, laser mirrors; 9, tiltable plate to control the role of the phase of the master laser; 10-11, mirrors; 12, $\lambda/2$ plate to control the polarization; 13-14-15, optical isolator.

equations, one for each component of the field, which are both considered as dynamical variables competing together in the case of a class-*A* laser. As the injected field is not resonant, the cavity losses associated with it are different from those of a resonant mode and vary with its frequency, as in an empty Fabry-Pérot cavity. We have thus introduced a different way of writing the basic equations. These two ideas—competing fields (leading to gain quenching) and frequency-dependent losses—when put together, give a harmonious model of the slave laser. We were able to compute the injected laser line shapes, whether or not the injected field frequency is tuned to line center. Theoretical results are obtained and compared to line shapes measured with a He-Ne laser operating at 3.39 μm. This comparison undoubtly proves the validity of our model, which also allows us to make the connection with the standard stability analysis. The locking range is thus defined in a standard way. We have tried to show the weaknesses of the traditional Adler model.

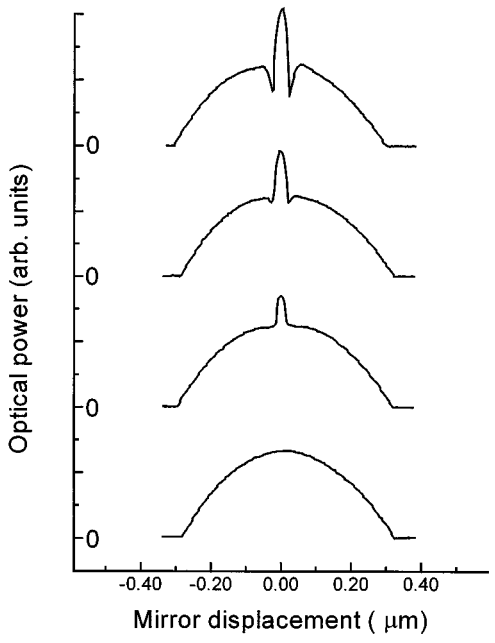

FIG. 9. Experimental SL line shape for increasing injection signal. X_2=0. Compare to Fig. 5.

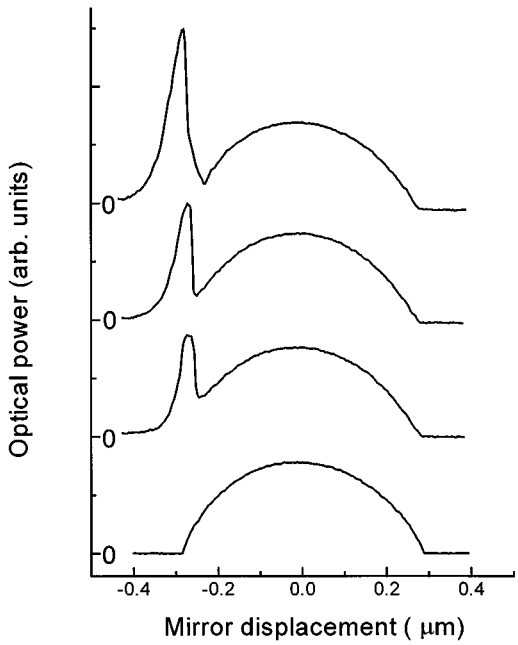

FIG. 10. Experimental SL line shape for increasing injection signal. X_2~0.3. Compare to Fig. 6.

We have obtained other theoretical and experimental results related to bistability effects. Up to now we have not yet measured them very precisely with our laser, but similar effects have been observed on semiconductor lasers and are well known by the specialists of the field [29]. Our ideas can be extended to these lasers by adding a dynamic equation for the injected field with the proper parameters to the set of equations that is normally used. They can also be extended to the vectorial case [22] or to the study of the dynamic properties of injected lasers [13]; our model contains the physics of the dispersive optical bistability and finally it is closely related to the theory of the laser linewidth [21], where the source term is spontaneous emission only.

ACKNOWLEDGMENTS

The optical isolator was kindly lent to us by N. B. Abraham (BrynMawr College). We have benefited from discussions with him and with Dr. Sanchez, Dr. Meziane, and Dr. Besnard.

APPENDIX A

The aim of this appendix is to give expressions for the gain and saturation coefficients and also to give the normalization coefficient for the intensity. We use the usual iteration-perturbation method applied to the density-matrix elements. The third-order polarizability is deduced from this calculation. This calculation has already been performed in Ref. [30], for instance, following standard methods.

The usual two energy levels are considered in the context of the dipolar approximation. H_0 represents the nonperturbed Hamiltonian, $\vec{\mu}$ is the dipolar moment, and $\vec{E}$ represents the field, which is written as a sum of the frequency components ω_1 and ω_2. The polarizability α_{ip} for each component E_i can be written

$$\alpha_{1p}=-\frac{S_0N_0}{\hbar ku}\,Z^*(\zeta_1)+\frac{N_0}{\hbar^3k^3u^3}\,(S_1+S_2+S_3)\times\left\{I_1\,\frac{1}{Y}\,iU_1^*+I_2\left[iV_{12}^*\,\frac{1}{Y}-W_{12}^*\,\frac{1}{X_2-X_1+iY}\right]\right\},$$

$$\alpha_{2p}=-\frac{S_0N_0}{\hbar ku}\,Z^*(\zeta_2)+\frac{N_0}{\hbar^3k^3u^3}\,(S_1+S_2+S_3)\times\left\{I_2\,\frac{1}{Y}\,iU_2^*+I_1\left[iV_{21}^*\,\frac{1}{Y}-W_{21}^*\,\frac{1}{X_1-X_2+iY}\right]\right\}.$$

The following symbols are used in these expressions:

$$S_0=\sum_m\,|\mu_{bm\pm1,am}|^2,$$

$$S_1=\sum_m\,|\mu_{bm\pm1,am}|^4,$$

$$S_2=\sum_m\,|\mu_{bm\pm1,am}|^2|\mu_{bm\pm1,am\pm2}|^2,$$

$$S_3=\sum_m\,|\mu_{bm\pm1,am}|^2|\mu_{bm\mp1,am}|^2.$$

These are sums over powers of matrix elements of the dipolar moments. For the 3.39-μm Ne line, one has the reduced sums

$$S_1=46|\mu_{ab}|^4,\quad S_2=21|\mu_{ab}|^4,\quad S_3=|\mu_{ab}|^4.$$

Functions U, V, and W are velocity integrals. They are expressed as functions of the plasma dispersion function Z [23],

$$U_1=Z_1'-\frac{Z_1}{\zeta_1}-\frac{Z_1^i}{Y}+\frac{Z_1^r}{X_1},\quad U_2=Z_2'-\frac{Z_2}{\zeta_2}-\frac{Z_2^i}{Y}+\frac{Z_2^r}{X_2},$$

$$V_{ij}=\frac{Z_i-Z_j}{X_i-X_j}-\frac{Z_i+Z_j}{X_i+X_j+2iY}-\frac{Z_i-Z_j^*}{X_i-X_j+2iY}+\frac{Z_i+Z_j^*}{X_i+X_j},$$

$$W_{ij}=Z_i'-\frac{Z_i}{X_i+iY}-\frac{Z_i-Z_j^*}{X_i-X_j+2iY}+\frac{Z_i+Z_j^*}{X_i+X_j}.$$

X_1 and X_2 are the detunings: $X_i=(\omega_i-\omega_0)/ku$ normalized by ku, which is half the inhomogeneous linewidth. Y is the ratio of the homogeneous over the inhomogeneous width. Typically $Y=0.5$. One has $\zeta_i=X_i+iY$; N_0 is the population inversion. I_1 and I_2 are the intensities of the field components. Pumping is defined with respect to threshold, which is itself defined in such a way that for this gain, losses are exactly compensated at line center. Thus one writes

$$\frac{\omega_0d_0}{\varepsilon_0c}\,\frac{S_0N_{0\mathrm{th}}}{\hbar ku}\,Z_0^i=\ln\left[\frac{1}{r_1r_2}\right]=p.$$

iZ_0^i is the value of Z for $X=0$. This relation defines $N_{0\mathrm{th}}$, the population inversion at threshold. A normalized polarizability for both components of the field can thus be written

$$\rho_1=pg\left\{-\frac{Z^*(\zeta_1)}{Z_0^i}+\left(\frac{S_1+S_2+S_3}{\hbar^2k^2u^2S_0Z_0^i}\right)\times\left(I_1\,\frac{1}{Y}\,iU_1^*+I_2\left[iV_{12}^*\,\frac{1}{Y}-W_{12}^*\,\frac{1}{X_2-X_1+iY}\right]\right)\right\},$$

$$\rho_2=pg\left\{-\frac{Z^*(\zeta_2)}{Z_0^i}+\left(\frac{S_1+S_2+S_3}{\hbar^2k^2u^2S_0Z_0^i}\right)\times\left(I_2\,\frac{1}{Y}\,iU_2^*+I_1\left[iV_{21}^*\,\frac{1}{Y}-W_{21}^*\,\frac{1}{X_1-X_2+iY}\right]\right)\right\}.$$

The normalization factor for intensities follows:

$$I_r=I_s(\omega_0)=\frac{S_0\hbar^2k^2u^2yZ_0^i}{(S_1+S_2+S_3)U_0^r}.$$

Here the subscript 0 means that the quantities are evaluated at line center and the superscripts i and r stand, respectively, for the imaginary and real parts of the complex functions. Finally, polarizabilities can be written under the more compact form

$$\rho_1=pg\{\alpha_1-\beta_1I_1-\theta_{12}I_2\},$$

$$\rho_2=pg\{\alpha_2-\beta_2I_2-\theta_{21}I_1\},$$

with the abbreviations for the normalized quantities, including the (negative) self- and cross-saturating terms:

$$\alpha_1=-\frac{Z^*(\zeta_1)}{Z_0^i},\quad \alpha_2=-\frac{Z^*(\zeta_2)}{Z_0^i},$$

$$\beta_1=-\frac{iU_1^*}{U_0^r},\quad \beta_2=-\frac{iU_2^*}{U_0^r},$$

$$\theta_{12}=-\left[iV_{12}^*-W_{12}^*\frac{y}{X_2-X_1+iY}\right]\frac{1}{U_0^r},$$

$$\theta_{21}=-\left[iV_{21}^*-W_{21}^*\frac{y}{X_1-X_2+iY}\right]\frac{1}{U_0^r}.$$

I_1 and I_2 now stand for intensities normalized by I_r.

APPENDIX B

The aim of this appendix is to give a few details on the calculations leading to the theoretical curves represented in Figs. 1–7. The system of equations (23) is first solved for the stationary solutions in cases A and B, i.e., with one or both components of the field. Then a small signal stability analysis is performed that shows the bistable regions and the hysteresis domains.

The system of equations (23) writes

$$\dot{\varepsilon}_1=\,=-\varepsilon_1[1-e^{-p+\rho_1^i}],$$

$$\dot{\varphi}_1=0,$$

$$\dot{\varepsilon}_2=\,=-\varepsilon_2[1-\cos(\Phi_2)e^{-p+\rho_2^i}]+\sqrt{T\eta}\,\cos(\varphi_2),$$

$$\dot{\varphi}_2=-\sin(\Phi_2)e^{-p+\rho_2^i}-\frac{\sqrt{T\eta}}{\varepsilon_2}\sin(\varphi_2).$$

One writes the dynamic variables in the form

$$\varepsilon_1=\varepsilon_{1s}+\delta\varepsilon_1,\quad \varepsilon_2=\varepsilon_{2s}+\delta\varepsilon_2,$$

where the index s stands for the stationary solutions and the symbols beginning with δ stand for small variations around these stationary values. One thus obtains the linearized equations of evolution of the small variations

$$\delta\dot{\varepsilon}_1=-\delta\varepsilon_1[1-(1+2pg\beta_1^iI_{1s})e^{-p+\rho_{1s}^i}]+\delta\varepsilon_2 2pg\varepsilon_{1s}\varepsilon_{2s}\theta_{12}^ie^{-p+\rho_{1s}^i},$$

$$\delta\dot{\varphi}_1=0,$$

$$\delta\dot{\varepsilon}_2=-\delta\varepsilon_2[1-\cos(\Phi_{2s})e^{-p+\rho_{2s}^i}]-\varepsilon_{2s}[\delta(\Phi_2)\sin(\Phi_{2s})e^{-p+\rho_{2s}^i}-\delta\rho_2^i\cos(\Phi_{2s})e^{-p+\rho_{2s}^i}]-\sqrt{T\eta}\,\sin(\varphi_{2s})\delta\varphi_2,$$

$$\delta\dot{\varphi}_2=-[\delta(\Phi_2)\cos(\Phi_{2s})e^{-p+\rho_{2s}^i}+\delta\rho_2^i\sin(\Phi_{2s})e^{-p+\rho_{2s}^i}]+\frac{\sqrt{T\eta}\,\sin(\varphi_2)}{\varepsilon_{2s}^2}\delta\varepsilon_2-\frac{\sqrt{T\eta}}{\varepsilon_{2s}}\delta\varphi_2\cos(\varphi_{2s}).$$

I_{1s} and I_{2s} are the stationary intensities, i.e., $I_{1s}=\varepsilon_{1s}\varepsilon_{1s}^*$ and $I_{2s}=\varepsilon_{2s}\varepsilon_{2s}^*$. This system can be written under a 3×3 matrix form that can be diagonalized in order to obtain the Lyapunov exponents.

Let us consider solution A first. This solution is characterized by

$$\varepsilon_{1s}=0,\quad \varepsilon_{2s}\neq0.$$

If we define the vector $\delta\vec{U}\equiv(\delta\varepsilon_1,\delta\varepsilon_2,\delta\varphi_2)$, the rate equation for $\delta\vec{U}$ can be written

$$\frac{d\,\delta\vec{U}}{dt}=M_A\delta\vec{U},$$

with

$$M_A=\begin{bmatrix}A_{11}&A_{12}&A_{13}\\A_{21}&A_{22}&A_{23}\\A_{31}&A_{32}&A_{33}\end{bmatrix},$$

where

$$A_{11}=-(1-e^{-p+\rho_{1s}^i}),\quad A_{12}=0,\quad A_{13}=0,\quad A_{21}=0,$$

$$A_{22}=-[1-\cos(\Phi_{2s})e^{-p+\rho_{2s}^i}]-2pgI_{2s}e^{-p+\rho_{2s}^i}[\beta_2^r\sin(\Phi_{2s})-\beta_2^i\cos(\Phi_{2s})],$$

$$A_{23}=-\sqrt{T\eta}\,\sin(\varphi_2),\quad A_{31}=0,$$

$$A_{32}=\frac{\sqrt{T\eta}}{\varepsilon_{2s}^2}\sin(\varphi_{2s})-2pg\varepsilon_{2s}[\beta_2^r\cos(\Phi_{2s})+\beta_2^i\sin(\Phi_{2s})]e^{-p+\rho_{2s}^i},$$

$$A_{33}=-\frac{\sqrt{T\eta}}{\varepsilon_{2s}}\cos(\varphi_{2s}).$$

We have used the abbreviations

$$\rho_{2s}=pg[\alpha_2-\beta_2I_{2s}],$$

$$\rho_{1s}=pg[\alpha_1-\theta_{12}I_{2s}],$$

$$2\Phi_{2s}=\frac{4\pi}{\lambda_0}\,\delta d+aX_2+\rho_{2s}^r.$$

In the case of solution B, both components of the field are different from zero: $\varepsilon_{1s}\neq0$ and $\varepsilon_{2s}\neq0$. In matrix form, one has again $d\,\delta\vec{U}/dt=M_B\delta\vec{U}$, with

$$M_B=\begin{bmatrix}B_{11}&B_{12}&B_{13}\\B_{21}&B_{22}&B_{23}\\B_{31}&B_{32}&B_{33}\end{bmatrix},$$

where

$$B_{11}=2pg\beta_1^iI_{1s},$$

$$B_{12}=2pg\varepsilon_{1s}\varepsilon_{2s}\theta_{12}^ie^{-p+\rho_{1s}^i},$$

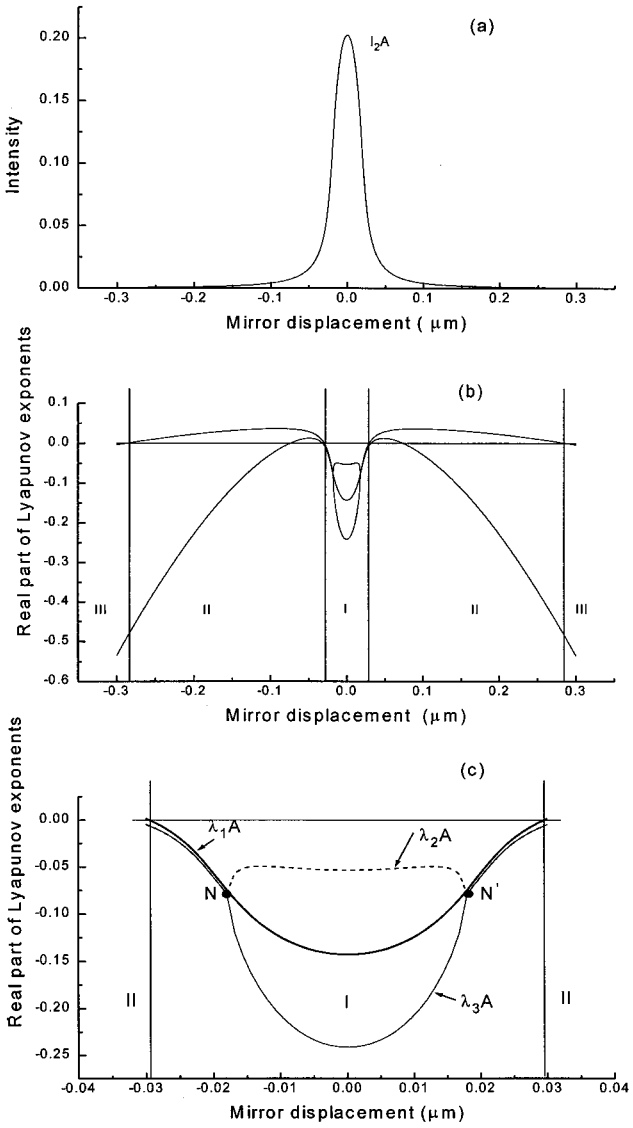

FIG. 11. Theoretical curves showing (a) the intensity I_{2A} inside the slave laser vs its length, (b) the Lyapunov coefficients associated with the solution A, and (c) a zoom of the central part of the curve for the Lyapunov coefficients. In the numerical calculation, we took $Y=0.5$, $d_0=45$ cm, $X_2=0$, and $\eta=0.04$. These values have been used in the calculation leading to this figure and Fig. 12.

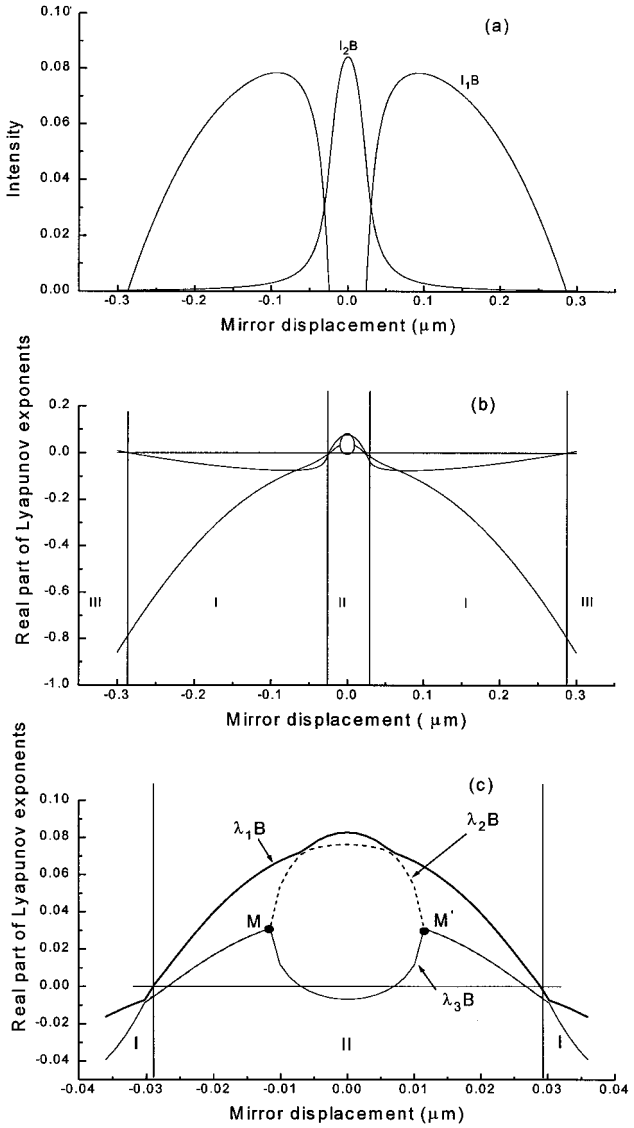

FIG. 12. Theoretical curves showing (a) the intensities I_{1B} and I_{2B} in the unlocked regime, inside the slave laser as a function of its length, (b) the Lyapunov coefficients associated with the solution B, and (c) a zoom of the central part of the curve for the Lyapunov coefficients.

$$B_{13}=0,$$

$$B_{21}=-2pg\varepsilon_{2s}\varepsilon_{1s}e^{-p+\rho_{2s}^{i}}[(\theta_{21}^{r}-\beta_1^{r})\sin(\Phi_{2s})-\theta_{21}^{i}\cos(\Phi_{2s})],$$

$$B_{22}=-[1-\cos(\Phi_{2s})e^{-p+\rho_{2s}^{i}}]-2pgI_{2s}e^{-p+\rho_{2s}^{i}}\times[(\beta_2^{r}-\theta_{12}^{r})\sin(\Phi_{2s})-\beta_2^{i}\cos(\Phi_{2s})],$$

$$B_{23}=-\sqrt{T}\eta\,\sin(\varphi_2),$$

$$B_{31}=-2pg\varepsilon_{1s}[(\theta_{21}^{r}-\beta_1^{r})\cos(\Phi_2)+\theta_{21}^{i}\sin(\Phi_2)],$$

$$B_{32}=\left[\frac{\sqrt{T}\eta}{\varepsilon_{2s}^{2}}\sin(\varphi_{s2})-2pg\varepsilon_{2s}[(\beta_2^{r}-\theta_{12}^{r})\cos(\Phi_{2s})+\beta_2^{i}\sin(\Phi_{2s})]\right]e^{-p+\rho_{s2}^{i}},$$

$$B_{33}=-\frac{\sqrt{T}\eta}{\varepsilon_{2s}}\cos(\varphi_{2s}),$$

with the abbreviations

$$\rho_{2s}=pg[\alpha_2-\beta_2 I_{2s}-\theta_{21}I_{1s}],$$

$$\rho_{1s}=pg[\alpha_1-\beta_1 I_{1s}-\theta_{12}I_{2s}],$$

$$2\Phi_{2s}=\rho_{2s}^{r}-\rho_{1s}^{r}+a(X_2-X_1).$$

Now the matrices M_A and M_B are diagonalized in order to study the stability of each solution belonging to cases A and B. Each solution is thus characterized by a set formed by the three eigenvalues, i.e., the Lyapunov exponents. For a solution to be stable, the real part of these three eigenvalues must be negative. The calculation is done by a computer. Cases A and B are illustrated in Figs. 11 and 12, respectively, where stationary solutions, together with their associated Lyapunov exponents, are drawn versus the mirror displacement of the slave laser and for $\eta=0.04$. Figure 11(a) represents I_{1B} and I_{2B} and Fig. 11(b) the associated real part of Lyapunov exponents noted λ_{1B}, λ_{2B}, and λ_{3B}. Figure 11(c) shows an enlarged version of Fig. 11(b) in the central zone. Equivalent curves for case A are drawn in Fig. 12(a), 12(b), and 12(c) with the evident notation λ_{1A}, λ_{2A}, and λ_{3A}.

One sees that for this value of the injection coefficient, the stability of both solutions is complementary, i.e., when solution A is unstable, solution B is stable and vice versa. The central zone where solution A is stable corresponds to the locking zone. From these data, it is possible to study independently the fields E_1 and E_2. On sees that in case B, the real part of the Lyapunov coefficient λ_{2B} and λ_{3B} are not degenerate between the limits labeled M and M'. The three coefficients are all different in this area. The same remark applies to the region limited by N and N' in case A. Finally, let us remind the reader that this example corresponds to the simple situation where there is only one real solution in both cases A and B. In the region where I_{2A}, or I_{1B} and I_{2B} are S shaped, one has three solutions for a given value of η. The calculations can become very long, especially if one has to converge toward the proper frequency linked to I_{2A}, or I_{1B} and I_{2B}.

[1] R. Adler, Proc. IEEE **61**, 1380 (1973) [reprinted from Proc. IRE **34**, 351 (1946)].

[2] C. J. Buczek, R. J. Freiberg, and M. L. Skolnick, J. Appl. Phys. **42**, 3133 (1971); C. J. Buczek and R. J. Freiberg, IEEE J. Quantum Electron. **QE-8**, 641 (1972).

[3] Pampaloni and Lapucci, Opt. Lett. **18**, 1881 (1993).

[4] W. W. Chow, IEEE J. Quantum Electron. **QE-19**, 243 (1983).

[5] C. N. Man and X. Brillet, Opt. Lett. **9**, 333 (1984).

[6] J. D. C. Jones and P. Urquhart, Opt. Commun. **76**, 42 (1990).

[7] H. L. Stover and W. H. Steier, Appl. Phys. Lett. **8**, 91 (1966).

[8] B. Couillaud, A. Ducasse, E. Freysz, and L. Sarger, Opt. Lett. **9**, 435 (1984).

[9] C. D. Nabors, A. D. Farinas, T. Day, S. T. Yang, E. K. Gustafson, and R. L. Byer, Opt. Lett. **14**, 1189 (1989).

[10] E. Gelmini, U. Minoni, and F. Docchio, Rev. Sci. Instrum. **66**, 4073 (1995).

[11] G. H. M. V. Tartwijk, and D. Lenstra, Quantum Semiclass. Opt. **7**, 87 (1995).

[12] A. E. Siegman, *Lasers* (University Science Books, Mill Valley, CA, 1986), Chap. 29.

[13] J. R. Tredicce, F. T. Arecchi, G. L. Lippi, and G. P. Pucioni, J. Opt. Soc. Am. B **2**, 173 (1985).

[14] G. P. Agrawal and G. R. Gray, Phys. Rev. A **46**, 5890 (1992).

[15] C. L. Tang and H. Statz, J. Appl. Phys. **38**, 323 (1967).

[16] R. F. Boikova and E. E. Fradkin, Opt. Spektrosk. **22**, 834 (1967) [Opt. Spectrosc. **22**, 452 (1967)].

[17] Y. K. Park, G. Guiliani, and R. L. Byer, IEEE J. Quantum Electron. **QE-20**, 117 (1984).

[18] P. Cassard and J. M. Lourtioz, IEEE J. Quantum Electron. **QE-24**, 2321 (1988).

[19] Hua Li, T. L. Lucas, J. G. McInerney, M. W. Wright, and R. A. Morgan, IEEE J. Quantum Electron. **QE-32**, 227 (1996).

[20] G. H. M. van Tartwijk, G. Muijres, D. Lenstra, M. P. van Exter, and J. P. Woerdman, Electron. Lett. **29**, 137 (1993).

[21] G. Stephan (unpublished).

[22] G. Ropars, A. Le Floch, and R. Le Naour, J. Opt. Soc. Am. **10**, 516 (1993). See Figs. 4 and 5 therein.

[23] M. B. Spencer and W. E. Lamb, Phys. Rev. A **5**, 884 (1972).

[24] M. B. Spencer and W. E. Lamb, Phys. Rev. A **5**, 893 (1972).

[25] K. Ujihara, IEEE J. Quantum Electron. **QE-20**, 814 (1984).

[26] S. Prasad, Phys. Rev. A **46**, 1540 (1992).

[27] C. D. Nabors, A. D. Farinas, T. Day, S. T. Yang, E. K. Gustafson, and R. L. Byer, Opt. Lett. **14**, 1189 (1989).

[28] P. Even, 3rd cycle thesis, University of Rennes, 1997 (unpublished).

[29] H. Kawaguchi, *Bistabilities and Nonlinearities in Laser Diodes* (Artech, Boston, 1994). See Sec. 4.2, p. 121, where hysteretic domains are described. G. Stephan thanks Dr. C. Salomon for showing him such an experimental hysteretic domain.

[30] A. D. May and G. Stephan, J. Opt. Soc. Am. **6**, 2355 (1989).